

Valley and spin polarized broken symmetry states of interacting electrons in gated MoS₂ quantum dots

Ludmiła Szulakowska,¹ Moritz Cygorek,¹ Maciej Bieniek,^{1,2} and Paweł Hawrylak¹

¹*Department of Physics, University of Ottawa, Ottawa, Ontario, Canada K1N 6N5*

²*Department of Theoretical Physics, Wrocław University of Science and Technology,
Wybrzeże Wyspiańskiego 27, 50-370 Wrocław, Poland*

(Dated: March 14, 2024)

Understanding strongly interacting electrons enables the design of materials, nanostructures and devices. Developing this understanding relies on the ability to tune and control electron-electron interactions by, e.g., confining electrons to atomically thin layers of 2D crystals with reduced screening. The interplay of strong interactions on a hexagonal lattice with two nonequivalent valleys, topological moments, and the Ising-like spin-orbit interaction gives rise to a variety of phases of matter corresponding to valley and spin polarized broken symmetry states. In this work we describe a highly tunable strongly interacting system of electrons laterally confined to monolayer transition metal dichalcogenide MoS₂ by metallic gates. We predict the existence of valley and spin polarized broken symmetry states tunable by the parabolic confining potential using exact diagonalization techniques for up to $N = 6$ electrons. We find that the ground state is formed by one of two phases, either both spin and valley polarized or valley unpolarised but spin intervalley antiferromagnetic, which compete as a function of electronic shell spacing. This finding can be traced back to the combined effect of Ising-like spin-orbit coupling and weak intervalley exchange interaction. These results provide an explanation for interaction-driven symmetry-breaking effects in valley systems and highlight the important role of electron-electron interactions for designing valleytronic devices.

I. INTRODUCTION

The role of electron-electron (e-e) interactions in determining the many-electron ground and excited states in different materials is controlled by the ratio of Coulomb energy V to kinetic energy T as $V/T = r_s$ where πr_s^2 is an area per electron¹. For small r_s electrons in 2D are well described by the Fermi liquid theory but as r_s increases, density decreases, and the spin polarised and Wigner crystal phases follow^{2,3}. In the 2D Hubbard model the electronic phases are controlled by the ratio of on-site Coulomb energy to the tunneling matrix element U/t . On a hexagonal lattice, calculations predict a semimetallic phase followed by the anti-ferromagnetic and Mott-insulating phase⁴⁻⁶. The U/t can be tuned by controlling screening (U) or controlling t . Recent work on twisted bilayer graphene (BG) showed that t can be significantly reduced by twisting layers in BG⁷. The quenching of tunneling results in strongly correlated system with Mott-insulating and superconducting phases^{8,9}. Recent experiments in BG^{10,11} and transition metal dichalcogenides (TMDCs) point to potential existence of spin¹² and valley polarized¹³ interaction driven broken symmetry valley and spin polarised states.

In this work we focus on a new emerging highly tunable strongly interacting system of N electrons laterally confined to monolayer 2D crystal, such as MoS₂,¹⁴⁻¹⁹ by metallic gates.²⁰⁻³⁴ The confinement to a single atomic layer leads to reduced screening and enhanced e-e interactions manifested in large, ~ 300 meV, exciton binding energies.^{16,32,35-37} Metallic gates can be used to define quantum dots (QDs) with discrete levels with spacings ω and enable a controlled charging of the QDs with N electrons. The ratio V/T scales with ω as $V/T = 1/\sqrt{\omega}$. In

small GaAs QDs at large ω , the ground state (GS) is well approximated by configurations minimizing single particle (SP) energy³⁸, but in large QDs, for small ω , spin polarised³⁸⁻⁴⁰ and correlated phases emerge^{38,41}. Here we combine the atomistic multimillion atom description of SP states, lateral confining potential and realistic e-e interaction matrix elements with accurate exact diagonalization techniques to determine GS and excited states of electrons in MoS₂ QDs.

II. MODEL

Fig. 1a shows the top view of a monolayer MoS₂ lattice. The blue (yellow) atoms correspond to Mo metal (S) atoms with 3 d -orbitals (3 p -orbitals) as described in detail in Ref.³³. The single particle (SP) Hamiltonian describes the tunneling of electrons between Mo d -orbitals and S p -orbitals. The conduction band (CB) wavefunctions are expanded in Mo and S orbitals and computed for a large computational box with $\sim 10^6$ atoms and periodic boundary conditions. The SP states are hence characterised by a band index and a wavevector \mathbf{k} , free from edge states present in a finite computational box. The relevant band structure consists of valence band (VB) and conduction band (CB), with the smallest energy gap at the two non-equivalent CB minima at $+K$ and $-K$ points of the Brillouin zone, and of six additional minima (3 per K -point), at the Q-points.

In such a realistic computational box we add a gate-defined parabolic confining potential $V(r)$ (described in V), as shown in Fig. 1b. The confining potential mixes the CB states, lowers their energy into the energy gap of MoS₂ and confines electrons to the center of a QD.

A schematic picture of a typical low energy SP spectrum is presented in Fig. 1c. It is doubly degenerate due to the valley index $+K, -K$. In each valley the spectrum resembles that of a 2D harmonic oscillator (HO), consisting of shells of states separated by the spacing ω , which can be tuned by the depth of the confining potential or the radius of the QD.^{39,42} A separate six-fold degenerate HO-like spectrum originating from Q points is present at higher energies (not shown). These states are not occupied by electrons for the range of ω considered here and are not considered in what follows. The SP levels are labelled with quantum numbers p, σ , where $p = [(n, m), K]$ contains state index (n, m) and valley index $+K, -K$, and σ denotes spin. The (n, m) are HO quantum numbers, where $n + m$ determines the shell index and $L = n - m$ is the angular momentum of the state in valley $+K$ (left) or $-K$ (right). The spin-orbit induced Zeeman splitting Δ_{SO} between spins (\uparrow and \downarrow shown in red and blue respectively in Fig. 1c) is opposite for both valleys.

A further modification of a simple HO level structure is a topological splitting δ proportional to ω , exhibited by all electronic shells. This splitting arises from the valley topological moments in each valley. This results in opposite angular momentum L states as the lowest energy states in $+K$ and $-K$ valleys.

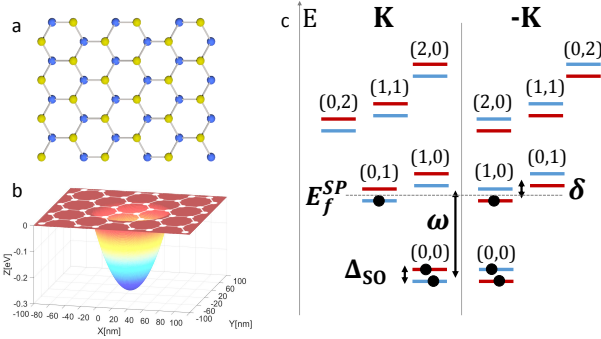


Figure 1. **MoS₂ quantum dots.** a. Rectangular computation box of monolayer MoS₂. Blue (yellow) atoms denote Mo (S) atoms. b. An example of the parabolic confining potential from the metallic gates with a depth of 300meV . White lattice represents the computation box in which electrons are confined to form a quantum dot (QD). c. Single-particle energy structure of an MoS₂ QD. The harmonic oscillator (HO) shells are doubly degenerate due to valleys K and $-K$. ω denotes shell spacing. Indices (n, m) label HO states. Spin down and up energy levels are split by the spin-orbit splitting Δ_{SO} , opposite in opposite valleys. HO shells are split by δ due to valley topological moments. To obtain a half-filling for 2 HO shells $N = 6$ electrons are needed. E_f^{SP} denotes the Fermi level for a non-interacting system of $N = 6$ electrons.

We next turn to filling SP spectrum with electrons up to the Fermi level E_f^{SP} , as illustrated in Fig. 1c) for $N = 6$ electrons. Our goal is to understand the many-

body GS and excited states of interacting electrons and explain how the interactions mix many configurations in forming correlated electronic states.

The many-body Hamiltonian in the basis of SP QD states reads

$$H = \sum_{p\sigma} e_{p\sigma} c_{p\sigma}^\dagger c_{p\sigma} + \frac{\eta}{2} \sum_{pqst\sigma\sigma'} \langle pq|V|st\rangle c_{p\sigma}^\dagger c_{q\sigma'}^\dagger c_{s\sigma'} c_{t\sigma}, \quad (1)$$

where the first term describes energies $e_{p\sigma}$ of the SP HO states $p\sigma$ shown in 1c) and the second term describes interaction energy, with Coulomb matrix elements describing scattering between pairs of states. The Coulomb matrix elements $\langle pq|V|st\rangle$ are computed using atomistic million atom orbitals and with both bare Coulomb and Keldysh-screened interaction^{43,44}, accounting for reduced screening by 2D materials [see V for details]. The parameter η allows us to turn the e-e interaction on and off.

The N -electron configurations are constructed as $|x\rangle = \prod_{p,\sigma} c_{p\sigma}^\dagger |0\rangle$, and the wavefunction of N -electron system is expanded in all possible electronic configurations $|x\rangle$. The Hamiltonian matrix in the space of configurations $|x\rangle$ is constructed and diagonalized giving exact eigenstates and eigenvalues. For example, for $N = 6$ we find up to $\sim 5 \cdot 10^7$ configurations for $M = 60$ SP orbitals.

We now turn to discuss the properties of N -electron systems. We focus here on $N = 2$, $N = 4$ and $N = 6$ electrons. This is because in a non-interacting system filling the first s-shell requires $N = 4$ electrons. Half filling of the s-shell is realised with $N = 2$ electrons and to obtain half filling of the first 2 shells $N = 6$ electrons are needed.

III. RESULTS

A. $N=2$ electron complex

In order to build the understanding of the role of interactions in MoS₂ QDs, it is instructive to first focus on $N = 2$ electrons on the first 4-fold degenerate s-shell of SP states. In the absence of SO splitting Δ_{SO} , this system describes the half-filled lowest energy shell of BG QD^{20,31,34} or a half-filled p-shell of a self-assembled QD³⁸. As we will see the GS is determined by the exchange interaction and can be understood in terms of spin singlets and triplets.

With $N = 2$ electrons on s-shell orbitals in opposite valleys the $N = 2$ electron spin states can be classified into three spin triplets $|T_+^s\rangle = |\uparrow\rangle|\uparrow\rangle$, $|T_0^s\rangle = \frac{1}{\sqrt{2}}(|\uparrow\rangle|\downarrow\rangle + |\downarrow\rangle|\uparrow\rangle)$, or $|T_-^s\rangle = |\downarrow\rangle|\downarrow\rangle$. The total wavefunction is therefore simultaneously a valley singlet $|S^v\rangle = \frac{1}{\sqrt{2}}(|K\rangle|-K\rangle - |-K\rangle|K\rangle)$. The spin triplet valley singlet state $|S^v\rangle|T_-^s\rangle$ is shown schematically in Fig. 2A. In the absence of Δ_{SO} , the energy of the spin triplet configuration E_T is composed of the sum of SP energies of s-type $(0,0)$ orbitals, the direct interaction V_D^0 and intervalley exchange $V_X^0(+K, -K)$ to give

$E_T = e_{00,\uparrow} + e_{00,\downarrow} + V_D^0(+K, -K) - V_X^0(+K, -K)$. The exchange interaction lowers the energy of $|T^s\rangle$ compared to $|S^s\rangle$. Exact diagonalisation of the $N = 2$ electron system on the lowest s-shell with $\Delta_{SO} = 0$ gives $|S^v\rangle|T^s\rangle$ as the triply degenerate GS, due to the intervalley exchange $V_X^0(+K, -K)$. This is in accordance with what has been found for half filled p-shell of QDs⁴⁵ and for BG QDs³¹, a two valley system with negligible SO.

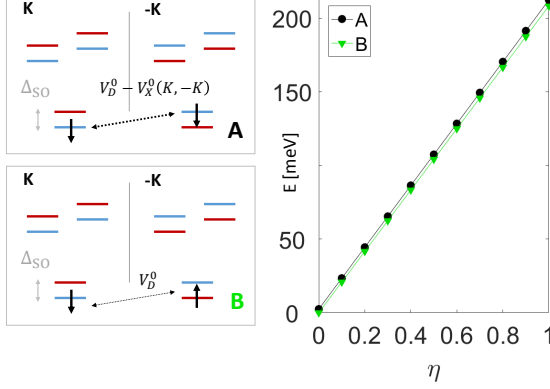


Figure 2. $N = 2$ electron configurations in the s-shell. Configurations A (spin polarised) and B (spin unpolarised) of $N = 2$ electrons in the s-shell are valley unpolarised. Two electrons in A interact with direct interaction V_D^0 and intervalley exchange $V_X^0(K, -K)$ (both include Keldysh screening), but have a higher single particle energy due to SO splitting Δ_{SO} . The electrons in B interact only with V_D^0 . The right panel shows the energies of A and B for increasing strength of interaction η . Due to much smaller intervalley exchange compared to SO splitting $V_X^0(K, -K) \ll \Delta_{SO}$, B has always lower energy. B makes up the many-body GS for $N = 2$ electrons in 1 shell, which is valley and spin unpolarised.

In TMDCs the Ising-like SO interaction leads to spin splitting in the CB ranging from $\sim 3\text{meV}$ in Mo-based material to $\sim 30\text{meV}$ in W-based material^{13,17}. Turning on Δ_{SO} leads to a decrease in the energy of spin-down states in valley K as well as of spin-up states in valley $-K$. For the case of $N = 2$ electrons this means that the spin triplets $|T^s\rangle$ and spin singlets $|S^s\rangle$ mix and the three-fold degeneracy of the $|S^v\rangle|T^s\rangle$ GS is broken by the Δ_{SO} . The splitting Δ_{SO} competes with intervalley exchange $V_X^0(+K, -K)$. For weak intervalley exchange $V_X^0(+K, -K) \ll \Delta_{SO}$ the spin unpolarized state, depicted as configuration B in Fig. 2, becomes the lower energy state separated by a gap from the spin polarized states, configuration A in Fig. 2. This is shown in Fig. 2 (right) for $\omega = 36\text{meV}$ and varied strength of Keldysh-screened Coulomb interactions η . Configuration B can be written as a mixture of $|S^v\rangle|T_0^s\rangle$ and $|T_0^v\rangle|S^s\rangle$ and becomes the spin-valley singlet $|S^{sv}\rangle = \frac{1}{\sqrt{2}}(|S^v\rangle|T_0^s\rangle - |T_0^v\rangle|S^s\rangle) = \frac{1}{\sqrt{2}}(|K\downarrow| -K\uparrow) - |-K\uparrow|K\downarrow\rangle$.

We now lower the level spacing ω and allow the second shell of p-type single-particle states to be occupied by a second electron, e.g. as shown in Fig. 3D and

Fig. 1C in Supplementary Material. The transfer from the s-shell to the p-shell costs SP energy $\omega + \delta/2$ but it is compensated by gain in interaction energy. Instead of $V_D^0(+K, -K) - V_X^0(+K, -K)$ for configuration A, the interaction is now $V_D^1(+K, +K) - V_X^1(+K, +K)$ (the superscript denotes L of the second electron). This change lowers the energy of D compared to A and B. This is because of the significantly stronger intra-valley exchange $V_X^1(+K, +K)$ compared to inter-valley $V_X^0(+K, -K)$. There are two possible p-shell orbitals and two possible $N = 2$ electron configurations, out of which D (with the second electron in $L = +1$ ($L = -1$) orbital at $+K$ ($-K$)) is lower in energy, as discussed in Supplementary Material.

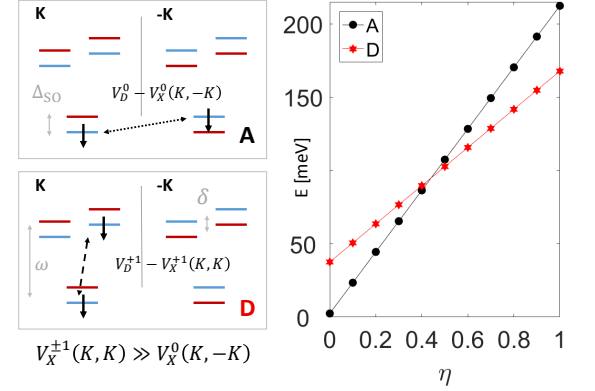


Figure 3. $N = 2$ electron configurations in 2 shells. Configurations A and D of $N = 2$ electrons are both spin polarised, with no valley polarisation in A and full valley polarisation in D. The electrons in A interact with intervalley exchange $V_X^0(+K, -K)$, while the electrons in D interact with much stronger intravalley exchange $V_X^1(K, K)$, which compensates the single-particle energy cost ω . These competing energies are responsible for generating an energy transition visible in the right panel as a function of the strength of interaction η . For a non-interacting case, at $\eta = 0$ A is lower in energy, but for an interacting system, D has lower energy.

This competition between configurations A and D is shown for $\omega = 36\text{meV}$ in Fig. 3 (right). For a non-interacting system, at $\eta = 0$, the valley and spin polarised configuration D with one electron on a p-shell has higher energy compared to valley unpolarised configuration A. However, as strength of interactions η is increased for Keldysh screened Coulomb interactions, we see a transition and the valley-spin polarised configuration D moves to lower energy. This transition can also be understood by considering the $N = 2$ electron wavefunction. Configuration D is a product of spin triplet $|T_-^s\rangle$, valley triplet $|T_-^v\rangle$ and hence electronic orbital s-p singlet $|S^e\rangle$, written as $|D\rangle = |S^e\rangle|T_-^{sv}\rangle$, where $|T_-^{sv}\rangle = |T_-^v\rangle|T_-^s\rangle$ (corresponding $|T_+^{sv}\rangle$ is degenerate). All other spin, valley and electronic orbital configurations can be constructed in a similar way, taking into account the nonzero Δ_{SO} (see Supplementary Materials for details). For higher shells D-

like configurations $|T_{-}^{sv}\rangle$ (valley-spin polarised) compete for the GS with the triplet configurations $|T_0^{sv}\rangle$ (valley-spin unpolarised).

B. GS and excited states of $N \geq 2$ and $M = 60$

We have so far identified different possible phases of the $N = 2$ electron system and different interactions competing to produce the GS and excited states: SP energies, SO splitting, topological moments, direct and exchange intravalley and intervalley interactions. We now describe results of exact diagonalisation of the $N = 2 - 6$ electron problem as a function of ω for varying number of electronic shells. Converged results for 5 shells per valley ($M = 60$ SP states) for $N = 2$ and $N = 6$ electrons are discussed below and remaining electron numbers are discussed in Supplementary Material. All our numerical results show spin valley locking in the many-body GS, with spin \uparrow (\downarrow) electrons occupying valley $+K$ ($-K$) so that $N_{\downarrow} = N_K$ and $N_{\uparrow} = N_{-K}$, which is in line with our explanation of the GS of the $N = 2$ -electron system. This allows us to label the GS with one polarisation quantum number $\tilde{V} = \frac{N_K - N_{-K}}{N}$, denoting total valley polarisation and equal here to the total spin polarisation $\tilde{V} = S_z \frac{2}{N} = \frac{N_{\uparrow} - N_{\downarrow}}{N}$.

The results for valley and spin polarisation \tilde{V} for $N = 2$ and $N = 6$ electrons are shown in the top panel of Fig. 4 while the corresponding energy gaps, $\Delta E_{X-GS} = E_X - E_{GS}$ where E_X is the first excited state, and schematic electron configurations are shown in the lower panel.

The colors in Fig. 4 (top) denote the degree of polarisation \tilde{V} : orange depicts full spin and valley polarisation (SVP) with total $|S_z| = N/2$, while dark green identifies a fully inter-valley anti-ferromagnetic (IVAF) GS with total $S_z = 0$ ($N_{\uparrow} = N_{\downarrow}$) and no net valley polarisation ($N_K = N_{-K}$). Schematic configurations corresponding to IVAF and SVP phases are shown for both N . Clear phase transitions from the IVAF GS to the SVP GS accompanying the closure of energy gaps ΔE_{X-GS} at critical energy spacings $\omega_C \approx 9\text{meV}$ and $\omega_C \approx 8\text{meV}$ are visible for $N = 2$ and $N = 6$ electrons respectively. For $N = 2$, the phases IVAF and SVP correspond to the competing triplets $|T_0^{sv}\rangle$ and $|T_{\pm}^{sv}\rangle$ respectively.

In the insets of Fig. 3. we show a schematic representation of the two competing GS phases for $N = 2$ and $N = 6$ electrons with spin \uparrow (\downarrow) electrons shown with red up (blue down) arrows. IVAF (left) involves $N_{\uparrow} = N_{-K} = N_{\downarrow} = N_K = 1$ and $N_{\uparrow} = N_{-K} = N_{\downarrow} = N_K = 3$ for $N = 2$ and $N = 6$ respectively. The SVP phase (right) is fully polarised with $N = N_{\downarrow} = N_K = 2$ (and a degenerate time-reversed state with $N = N_{\uparrow} = N_{-K} = 2$) and similarly $N = N_{\downarrow} = N_K = 6$ (and a degenerate time-reversed state with $N = N_{\uparrow} = N_{-K} = 6$).

In order to detect the competing GS phases in an experiment, one needs to consider the stability of these phases. It is partly determined by the energy spacing be-

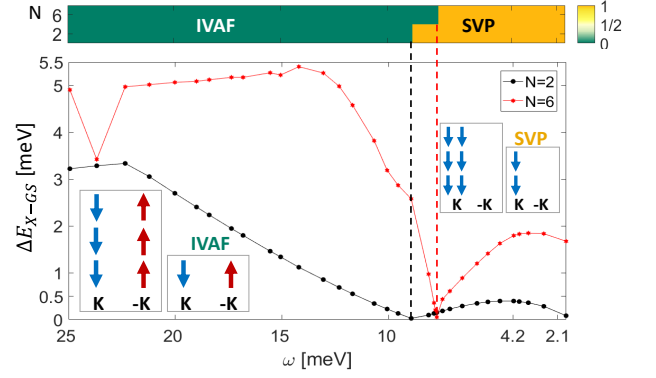


Figure 4. Transition in the many-body ground state character with varying level spacing ω . The top panel shows the nature of the ground state (GS) for $N = 2$ and $N = 6$ electrons as a function of the HO shell spacing ω . Colors depict the polarisation quantum number \tilde{V} (see text for details): dark green depicts the intervalley antiferromagnetic (IVAF) GS while orange stands for spin and valley polarised (SVP) GS. The bottom panel contains the energy difference ΔE_{X-GS} between the GS and the first excited state for varying ω for $N = 2$ (black dots) and $N = 6$ (red stars). Vanishing ΔE_{X-GS} marks a transition in the nature of the GS from the IVAF to the SVP phase (shown with dashed lines). Insets give schematic representation of the IVAF and the SVP GS phases (red and blue arrows depict spin up and down).

tween the GS and excited state ΔE_{X-GS} , which in turn impacts transport measurement. Closing of the energy gaps due to phase transitions would affect the temperature dependence and high-source-drain Coulomb diamonds in transport. The computed energy gaps ΔE_{X-GS} as a function of ω for $N = 2$ (black) and $N = 6$ (red) reach several meV. The quantum phase transitions between IVAF and SVP phases occur when $\Delta E_{X-GS} = 0$.

IV. CONCLUSIONS

Using atomistic theory combined with exact many-body diagonalisation tools we predict the existence of broken-symmetry Spin and Valley Polarized (SVP) and InterValley AntiFerromagnetic (IVAF) electronic states of interacting electrons electrostatically confined in a parabolic QD in a single layer of MoS_2 . These results highlight the important role of electron-electron interactions for designing valleytronic devices.

V. METHODS

The hexagonal MoS_2 layer consists of two triangular lattices, one of Mo atoms and a second of S_2 dimer. We write our Hamiltonian in the basis of d orbitals of Mo atoms and p orbitals of S_2 dimers, which are even with

respect to the metal plane, as³³

$$\hat{H}^{TB} = \sum_i E_i c_i^\dagger c_i + \sum_{\langle i,j \rangle} \left(T_{ij} c_i^\dagger c_j + h.c. \right) + \sum_{\langle\langle i,j \rangle\rangle} \left(W_{ij} c_i^\dagger c_j + h.c. \right), \quad (2)$$

where c_i^\dagger creates an electron on state i , and i carries atom unit cell index, orbital index and sublattice index. E_i are onsite energies and T (W) are 6×6 nearest neighbour (NN) (next nearest neighbour (NNN)) hopping matrices between sites. Energies E_i include the parabolic potential V_i generated by the gates (as shown in Fig. 1 b)) on a site corresponding to index i , with $V_i = V(\mathbf{r}_i) = |V_{max}| / (R_{QD}^2 \cdot \mathbf{r}_i^2 - V_{max})$, for $|\mathbf{r}_i| \leq R_{QD}$ and 0 elsewhere. V_{max} is the depth of the potential and R_{QD} is the radius of the QD.

To avoid edge states in the energy gap we apply periodic boundary conditions, i.e., we wrap the finite computational box on a torus with periodic boundary conditions. The Hamiltonian in Eq. (2) can now be written in the basis of Bloch states as

$$\begin{aligned} \hat{H}_{\mathbf{k}-basis}^{TB} = & \sum_{\mathbf{k}} \sum_{\alpha} E_{\alpha} a_{\mathbf{k}\alpha}^\dagger a_{\mathbf{k}\alpha} \\ & + \sum_{\mathbf{k}} \sum_{\langle \alpha, \beta \rangle} \left(e^{i\mathbf{k}\mathbf{d}_{\alpha,\beta}} T_{\alpha,\beta} a_{\mathbf{k}\alpha}^\dagger a_{\mathbf{k}\beta} + h.c. \right) \\ & + \sum_{\mathbf{k}} \sum_{\langle\langle \alpha, \beta \rangle\rangle} \left(e^{i\mathbf{k}\mathbf{d}_{\alpha,\beta}} W_{\alpha,\beta} a_{\mathbf{k}\alpha}^\dagger a_{\mathbf{k}\beta} + h.c. \right) \\ & + \sum_{\mathbf{k}, \mathbf{k}'} \sum_{\mathbf{R}, \alpha} \left(e^{i(\mathbf{k}-\mathbf{k}')\mathbf{R}} V_{\mathbf{R},\alpha} a_{\mathbf{k}\alpha}^\dagger a_{\mathbf{k}'\alpha} + h.c. \right), \quad (3) \end{aligned}$$

where \mathbf{R} is position of a cell and α carries orbital and sublattice index. $\mathbf{d}_{\alpha,\beta}$ is the NN or NNN vector between NN or NNN orbitals α, β , and only the confining potential $V_{\mathbf{R}\alpha}$ mixes the \mathbf{k} -states²¹.

We diagonalise Eq. (3) to obtain valley specific quantum dot states p, σ . In the second quantization the many-

body Hamiltonian in the basis of SP QD states p, σ reads:

$$H = \sum_{p\sigma} e_{p\sigma} c_{p\sigma}^\dagger c_{p\sigma} + \frac{\eta}{2} \sum_{pqst\sigma\sigma'} \langle pq|V|st \rangle c_{p\sigma}^\dagger c_{q\sigma'}^\dagger c_{s\sigma'} c_{t\sigma}, \quad (4)$$

where in the first term $e_{p\sigma}$ are energies of the SP HO states p and the second terms includes Coulomb scattering between these states, with η controlling the strength of the interactions. We express the Coulomb matrix elements $\langle pq|V|st \rangle$ in Eq. (4) in the basis of atomic orbitals as $\langle pq|V|st \rangle = \sum_{ijkl} A_i^{p*} A_j^{q*} A_k^s A_l^t \langle ij|V|kl \rangle$, where A are solutions to the SP Hamiltonian in Eq. (2) and Eq. (3). We include only onsite short-range integrals $\langle ii|V|ii \rangle$ and the long-range part is taken as a classical Coulomb term. The Coulomb integrals are calculated using Coulomb potential with Keldysh screening, using the 2D Fourier transform, as³⁷

$$V_K^{3D}(\mathbf{r} - \mathbf{r}') = \frac{1}{\epsilon^*} \frac{e^2}{4\pi\epsilon_0} \frac{1}{(2\pi)^2} \cdot \int_{-\infty}^{\infty} \frac{2\pi}{|\mathbf{k}|} \frac{1}{1 + 2\pi\alpha|\mathbf{k}|} e^{-|z-z'||\mathbf{k}|} e^{i\mathbf{k}(\boldsymbol{\rho}-\boldsymbol{\rho}')} d^2\mathbf{k}, \quad (5)$$

where $\alpha = 2.2\text{\AA}$ is the 2D polarisability and we take $\epsilon^* = 2.5$.

ACKNOWLEDGMENTS

L.S., M.C., M.B., and P.H. thank M. Korkusinski, Y. Saleem, A. Altintas, A. Dusko, J. Manalo, A. Luican-Mayer, A. Badolato, I. Ozfidan, L. Gaudreau, S. Studenikin and A. Sachrajda for discussions. L.S., M.C., M.B., and P.H. acknowledge support from NSERC Discovery and QC2DM Strategic Project grants as well as uOttawa Research Chair in Quantum Theory of Materials, Nanostructures and Devices. M.B. acknowledges financial support from National Science Center (NCN), Poland, grant Maestro No. 2014/14/A/ST3/00654. M.C. acknowledges support from the Humboldt Foundation. Computing resources from Compute Canada are gratefully acknowledged.

¹ Gabriele F. Giuliani and Giovanni Vignale, *Quantum theory of the Electron Liquid* (Cambridge University Press, New York, 2005).

² Claudio Attaccalite, Saverio Moroni, Paola Gori-Giorgi, and Giovanni B. Bachelet, “Correlation Energy and Spin Polarization in the 2D Electron Gas,” *Physical Review Letters* **88**, 256601 (2002).

³ M. Zarenia, D. Neilson, B. Partoens, and F. M. Peeters, “Wigner crystallization in transition metal dichalcogenides: A new approach to correlation energy,” *Physical Review B* **95**, 115438 (2017).

⁴ S Sorella and E Tosatti, “Semi-Metal-Insulator Transition of the Hubbard Model in the Honeycomb Lattice,” *Europhysics Letters (EPL)* **19**, 699–704 (1992).

⁵ Yuichi Otsuka, Seiji Yunoki, and Sandro Sorella, “Universal Quantum Criticality in the Metal-Insulator Transition of Two-Dimensional Interacting Dirac Electrons,” *Physical Review X* **6**, 011029 (2016).

⁶ T. O. Wehling, E. Şaşıoğlu, C. Friedrich, A. I. Lichtenstein, M. I. Katsnelson, and S. Blügel, “Strength of Effective Coulomb Interactions in Graphene and Graphite,” *Physical Review Letters* **106**, 236805 (2011).

- ⁷ A. Luican, Guohong Li, A. Reina, J. Kong, R. R. Nair, K. S. Novoselov, A. K. Geim, and E. Y. Andrei, "Single-Layer Behavior and Its Breakdown in Twisted Graphene Layers," *Physical Review Letters* **106**, 126802 (2011).
- ⁸ Yuan Cao, Valla Fatemi, Ahmet Demir, Shiang Fang, Spencer L. Tomarken, Jason Y. Luo, Javier D. Sanchez-Yamagishi, Kenji Watanabe, Takashi Taniguchi, Efthimios Kaxiras, Ray C. Ashoori, and Pablo Jarillo-Herrero, "Correlated insulator behaviour at half-filling in magic-angle graphene superlattices," *Nature* **556**, 80–84 (2018).
- ⁹ Yuan Cao, Valla Fatemi, Shiang Fang, Kenji Watanabe, Takashi Taniguchi, Efthimios Kaxiras, and Pablo Jarillo-Herrero, "Unconventional superconductivity in magic-angle graphene superlattices," *Nature* **556**, 43–50 (2018).
- ¹⁰ Kentaro Nomura and Allan H. MacDonald, "Quantum Hall Ferromagnetism in Graphene," *Physical Review Letters* **96**, 256602 (2006).
- ¹¹ R. T. Weitz, M. T. Allen, B. E. Feldman, J. Martin, and A. Yacoby, "Broken-Symmetry States in Doubly Gated Suspended Bilayer Graphene," *Science* **330**, 812–816 (2010).
- ¹² Jonas Gaël Roch, Guillaume Froehlicher, Nadine Leisgang, Peter Makk, Kenji Watanabe, Takashi Taniguchi, and Richard John Warburton, "Spin-polarized electrons in monolayer MoS₂," *Nature Nanotechnology* **14**, 432–436 (2019).
- ¹³ T. Scrase, Y. Tsai, B. Barman, L. Schweidenback, A. Petrou, G. Kioseoglou, I. Ozfidan, M. Korkusinski, and P. Hawrylak, "Magnetoluminescence and valley polarized state of a two-dimensional electron gas in WS₂ monolayers," *Nature Nanotechnology* **10**, 603–607 (2015).
- ¹⁴ A. K. Geim and I. V. Grigorieva, "Van der Waals heterostructures," *Nature* **499**, 419–425 (2013).
- ¹⁵ Andrea Splendiani, Liang Sun, Yuanbo Zhang, Tianshu Li, Jonghwan Kim, Chi-Yung Chim, Giulia Galli, and Feng Wang, "Emerging Photoluminescence in Monolayer MoS₂," *Nano Letters* **10**, 1271–1275 (2010).
- ¹⁶ Kin Fai Mak, Changgu Lee, James Hone, Jie Shan, and Tony F. Heinz, "Atomically Thin MoS₂: A New Direct-Gap Semiconductor," *Physical Review Letters* **105**, 136805 (2010).
- ¹⁷ Eugene S. Kadantsev and Pawel Hawrylak, "Electronic structure of a single MoS₂ monolayer," *Solid State Communications* **152**, 909–913 (2012).
- ¹⁸ Yang Yu, Jianchen Dang, Chenjiang Qian, Sibai Sun, Kai Peng, Xin Xie, Shiyao Wu, Feilong Song, Jingnan Yang, Shan Xiao, Longlong Yang, Yunuan Wang, Xinyan Shan, M. A. Rafiq, Bei-Bei Li, and Xiulai Xu, "Many-body effect of mesoscopic localized states in MoS₂ monolayer," *Physical Review Materials* **3**, 051001 (2019).
- ¹⁹ Dinh Van Tuan, Min Yang, and Hanan Dery, "Coulomb interaction in monolayer transition-metal dichalcogenides," *Physical Review B* **98**, 125308 (2018).
- ²⁰ C. Volk, S. Fringes, B. Terrés, J. Dauber, S. Engels, S. Trelenkamp, and C. Stampfer, "Electronic Excited States in Bilayer Graphene Double Quantum Dots," *Nano Letters* **11**, 3581–3586 (2011).
- ²¹ Gui-Bin Liu, Hongliang Pang, Yugui Yao, and Wang Yao, "Intervalley coupling by quantum dot confinement potentials in monolayer transition metal dichalcogenides," *New Journal of Physics* **16**, 105011 (2014).
- ²² Andor Kormányos, Viktor Zólyomi, Neil D. Drummond, and Guido Burkard, "Spin-Orbit Coupling, Quantum Dots, and Qubits in Monolayer Transition Metal Dichalcogenides," *Physical Review X* **4**, 011034 (2014).
- ²³ Alev Devrim Güçlü, Paweł Potasz, Marek Korkusinski, and Paweł Hawrylak, *Graphene quantum dots* (Springer-Verlag, Berlin, Heidelberg, 2014).
- ²⁴ Xiang-Xiang Song, Di Liu, Vahid Mosallanejad, Jie You, Tian-Yi Han, Dian-Teng Chen, Hai-Ou Li, Gang Cao, Ming Xiao, Guang-Can Guo, and Guo-Ping Guo, "A gate defined quantum dot on the two-dimensional transition metal dichalcogenide semiconductor WSe₂," *Nanoscale* **7**, 16867–16873 (2015).
- ²⁵ J. Pawłowski, D. Żebrowski, and S. Bednarek, "Valley qubit in a gated MoS₂ monolayer quantum dot," *Physical Review B* **97**, 155412 (2018).
- ²⁶ Riccardo Pisoni, Zijin Lei, Patrick Back, Marius Eich, Hiske Overweg, Yongjin Lee, Kenji Watanabe, Takashi Taniguchi, Thomas Ihn, and Klaus Ensslin, "Gate-tunable quantum dot in a high quality single layer MoS₂ van der Waals heterostructure," *Applied Physics Letters* **112**, 123101 (2018).
- ²⁷ S Bhandari, K Wang, K Watanabe, T Taniguchi, P Kim, and R M Westervelt, "Imaging quantum dot formation in MoS₂ nanostructures," *Nanotechnology* **29**, 42LT03 (2018).
- ²⁸ Ke Wang, Kristiaan De Greve, Luis A. Jauregui, Andrey Sushko, Alexander High, You Zhou, Giovanni Scuri, Takashi Taniguchi, Kenji Watanabe, Mikhail D. Lukin, Hongkun Park, and Philip Kim, "Electrical control of charged carriers and excitons in atomically thin materials," *Nature Nanotechnology* **13**, 128–132 (2018).
- ²⁹ Qiao Chen, L. L. Li, and F. M. Peeters, "Magnetic field dependence of electronic properties of MoS₂ quantum dots with different edges," *Physical Review B* **97**, 085437 (2018).
- ³⁰ J Pawłowski, "Spin-valley system in a gated MoS₂ - monolayer quantum dot," *New Journal of Physics* **21**, 123029 (2019).
- ³¹ A Kurzman, M Eich, H Overweg, M Mangold, F Herman, P Rickhaus, R Pisoni, Y Lee, R Garreis, C Tong, K Watanabe, T Taniguchi, K Ensslin, and T Ihn, "Excited States in Bilayer Graphene Quantum Dots," *PHYSICAL REVIEW LETTERS*, 5 (2019).
- ³² T. N. Lin, S. R. M. Santiago, S. P. Caigas, C. T. Yuan, T. Y. Lin, J. L. Shen, and Y. F. Chen, "Many-body effects in doped WS₂ monolayer quantum disks at room temperature," *npj 2D Materials and Applications* **3**, 46 (2019).
- ³³ Maciej Bieniek, Ludmiła Szulakowska, and Paweł Hawrylak, "Effect of valley, spin, and band nesting on the electronic properties of gated quantum dots in a single layer of transition metal dichalcogenides," *Physical Review B* **101**, 035401 (2020).
- ³⁴ Angelika Knothe and Vladimir Fal'ko, "Quartet states in two-electron quantum dots in bilayer graphene," *arXiv:2002.12845 [cond-mat, physics:quant-ph]* (2020), arXiv: 2002.12845.
- ³⁵ Diana Y. Qiu, Ting Cao, and Steven G. Louie, "Nonanalyticity, Valley Quantum Phases, and Light-like Exciton Dispersion in Monolayer Transition Metal Dichalcogenides: Theory and First-Principles Calculations," *Physical Review Letters* **115** (2015), 10.1103/PhysRevLett.115.176801.
- ³⁶ J. Jadczak, A. Delgado, L. Bryja, Y. S. Huang, and P. Hawrylak, "Robust high-temperature trion emission in monolayers of Mo (S y Se 1 - y)₂ alloys," *Physical Review*

- B **95** (2017), 10.1103/PhysRevB.95.195427.
- ³⁷ Maciej Bieniek, Ludmiła Szulakowska, and Paweł Hawrylak, “Band nesting and exciton spectrum in monolayer MoS₂,” *Physical Review B* **101**, 125423 (2020).
 - ³⁸ M. Korkusinski, W. Sheng, and P. Hawrylak, “Designing quantum systems in self-assembled quantum dots,” *physica status solidi (b)* **238**, 246–249 (2003).
 - ³⁹ Paweł Hawrylak, “Single-electron capacitance spectroscopy of few-electron artificial atoms in a magnetic field: Theory and experiment,” *Physical Review Letters* **71**, 3347–3350 (1993).
 - ⁴⁰ S. A. Mikhailov, “Quantum-dot lithium in zero magnetic field: Electronic properties, thermodynamics, and Fermi liquid–Wigner solid crossover in the ground state,” *Physical Review B* **65**, 115312 (2002).
 - ⁴¹ Marek Korkusiński, Paweł Hawrylak, Mariusz Ciorga, Michel Pioro-Ladrière, and Andrew S. Sachrajda, “Pairing of Spin Excitations in Lateral Quantum Dots,” *Physical Review Letters* **93**, 206806 (2004).
 - ⁴² S. Raymond, S. Studenikin, A. Sachrajda, Z. Wasilewski, S. J. Cheng, W. Sheng, P. Hawrylak, A. Babinski, M. Potemski, G. Ortner, and M. Bayer, “Excitonic Energy Shell Structure of Self-Assembled InGaAs/GaAs Quantum Dots,” *Physical Review Letters* **92**, 187402 (2004).
 - ⁴³ N. S. Rytova, “The screened potential of a point charge in a thin film,” *Moscow University Physics Bulletin* **3**, 18 (1967).
 - ⁴⁴ LV Keldysh, “Coulomb interaction in thin semiconductor and semimetal films,” *Soviet Journal of Experimental and Theoretical Physics Letters* **29**, 658 (1979).
 - ⁴⁵ Arkadiusz Wojs and Paweł Hawrylak, “Charging and infrared spectroscopy of self-assembled quantum dots in a magnetic field,” *Physical Review B* **53**, 10841–10845 (1996).